Functional Role of Loop 2 in Myosin V†

Christopher M. Yengo‡ and H. Lee Sweeney*

Department of Physiology, University of Pennsylvania School of Medicine, Philadelphia, Pennsylvania 19104

Received August 22, 2003; Revised Manuscript Received December 3, 2003

ABSTRACT: Myosin V is molecular motor that is capable of moving processively along actin filaments. The kinetics of monomeric myosin V containing a single IQ domain (MV 1IQ) differ from nonprocessive myosin II in that actin affinity is higher, phosphate release is extremely rapid, and ADP release is rate-limiting. We generated two mutants of myosin V by altering loop 2, a surface loop in the actin-binding region thought to alter actin affinity and phosphate release in myosin II, to determine the role that this loop plays in the kinetic tuning of myosin V. The loop 2 mutants altered the apparent affinity for actin (K_{ATPase}) without altering the maximum ATPase rate (V_{MAX}). Transient kinetic analysis determined that the rate of binding to actin, as well as the affinity for actin, was dependent on the net positive charge of loop 2, while other steps in the ATPase cycle were unchanged. The maximum rate of phosphate release was unchanged, but the affinity for actin in the M·ADP·Pi-state was dramatically altered by the mutations in loop 2. Thus, loop 2 is important for allowing myosin V to bind to actin with a relatively high affinity in the weak binding states but does not play a direct role in the product release steps. The ability to maintain a high affinity for actin in the weak binding states may prevent diffusion away from the actin filament and increase the degree of processive motion of myosin V.

Myosins make up a large superfamily of motor proteins that are capable of using the chemical energy from ATP hydrolysis to power the directed movement on actin filaments and function in a wide variety of cellular processes from muscle contraction to organelle transport (*1*). During the actomyosin ATPase cycle myosin shifts between actin-detached (weak-binding) and actin-attached states (strong-binding), and force generation occurs through a conformational change in myosin during the transition from the weak- to the strong-actin binding states (reviewed in ref *2*). Interestingly, the overall structure of myosin proteins appears to be quite conserved, while their biochemical and kinetic properties are quite divergent. It has been proposed that sequence variability in the two surface loops of myosin, which are susceptible to proteolysis and divide myosin into three domains (25, 50, and 20 kDa, Figure 1), may play a role in kinetically tuning a particular myosin to perform specific cellular functions (*3*−*6*). In the current study, we examine the role of loop 2, a surface loop in the actin-binding region of myosin, in kinetically tuning myosin V, a non-muscle myosin that functions as an organelle transporter.

Myosin V has several unique biochemical features that allow it to move processively along actin (*7*), take multiple steps along actin without diffusing away, and function as an organelle transporter (*8*). The kinetics of myosin V are different from nonprocessive muscle myosin II in that ADP release in myosin V is slow and rate-limiting, while phosphate release is fast (*9*−*11*). This allows myosin V to populate the strong-binding states for a greater fraction of its ATPase cycle and increase its duty ratio, fraction of ATPase cycle that myosin is strongly bound to actin. In a previous report, we determined that myosin V has a higher affinity for actin in the weak binding states (*12*) than nonprocessive class II myosins, which may also be an important aspect of its ability to move processively. Thus, the current study is focused on examining the structural aspects of myosin V that give rise to its high affinity for actin.

One unique structural feature of myosin V is that it has a large and highly charged surface loop, commonly referred

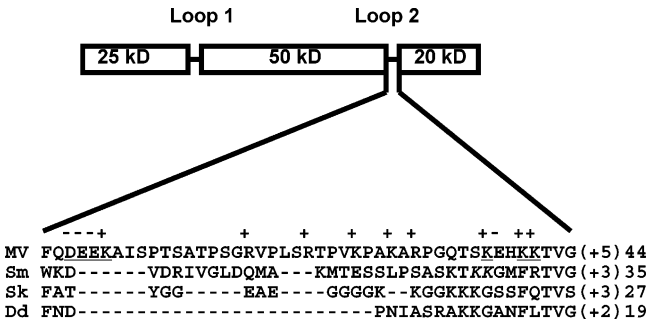

FIGURE 1: Alignment of myosin loop 2 sequences. The alignment of loop 2 sequences from chicken myosin V (MV), smooth muscle myosin II (Sm), skeletal muscle myosin II (Sk), and *Dictyolstelium* myosin II (Dd) is shown, along with the overall charge in parentheses and size of the loop 2 from each isoform. The lysine residues in myosin V that were substituted with alanines and the four residues that were deleted are underlined. Also the smooth muscle myosin lysines that were substituted with alanines are indicated in italics. The alignment was adapted from ref 1.

† This work was supported by a National Institute of Health Grant AR35661 (to H.L.S.).

* To whom correspondence should be addressed: Department of Physiology, A400 Richards Bldg., University of Pennsylvania School of Medicine, Philadelphia, PA 19104-6085. Tel: 215-898-0486. Fax: 215-898-0475. E-mail: lsweeney@mail.med.upenn.edu.

‡ A National Institute of Health NRSA Postdoctoral Fellow. Current address: Department of Biology, University of North Carolina at Charlotte.

10.1021/bi035510v CCC: $27.50
Published on Web 02/12/2004

to as loop 2, in its actin-binding region (see ref *1* for comparison of myosin isoforms). Studies examining the role of loop 2 in myosin II have determined that variability in the length and number of charged residues in this loop can alter myosin's affinity for actin, as well as its enzymatic activity (*4*, *13*−*17*). In addition, a study on smooth muscle myosin demonstrated that substituting two lysine residues in loop 2 completely blocked the actin-activated ATPase activity of this myosin, but a 16 amino acid deletion of the loop that retained the critical lysine residues actually increased smooth muscle myosin's affinity for actin (*18*). Alignment of loop 2 of myosin V with other myosin isoforms demonstrates a unique six amino acid insert in the N-terminal region as well as several positively charged residues in the C-terminal part of the loop (Figure 1). Therefore, it is unclear whether the unique features of loop 2 of myosin V are important for increasing affinity for actin or controlling actin activation of product release or both.

We examined the role of loop 2 in myosin V by performing a complete kinetic characterization of two mutants of myosin V with modified loop 2 sequences. We generated one mutant of myosin V with a single IQ binding motif (MV 1IQ) that had three lysine residues (residues 630, 633, 634) substituted with alanines (LP2AAA MV 1IQ) in the same region as the lysines that were substituted with alanines in the smooth muscle myosin study (*18*). We also generated a mutant with four amino acids deleted from the unique insert in the N-terminal region of loop 2 (residues Asp595, Glu596, Glu597, Lys598). In addition, we further examined the kinetic properties of a monomeric version (subfragment 1, S1) of a smooth muscle myosin mutant with two lysine residues substituted with alanines, which was previously examined in a dimeric heavy meromyosin (HMM) background (*18*), to directly compare it to our myosin V loop 2 mutants. Our results suggest a structural role for loop 2 in allowing myosin V to bind to actin with a relatively high affinity in the weak binding states compared to myosin II, while not altering other steps in the catalytic cycle of myosin V.

EXPERIMENTAL PROCEDURES

Reagents. All reagents were the highest purity commercially available. ATP was prepared fresh from powder (Roche Molecular Biochemicals, 99.7% pure by HPLC (data not shown). *N*-Methylanthraniloyl (mant)-labeled ADP and ATP were prepared as described (*19*). ATP and ADP concentrations were determined by absorbance at 259 nm using ϵ_{259} of 15 400 $M^{-1}\cdot cm^{-1}$. Nucleotides were prepared prior to use in the presence of equimolar $MgCl_2$.

Myosin cDNA Construction and Protein Expression and Purification. Site-directed mutagenesis was performed on a construct of chicken myosin V containing a single IQ motif (WT MV 1IQ) (residues 1−792). We substituted three lysine residues in loop 2 (630, 633, and 634) with alanines to generate the LP2AAA MV 1IQ construct, and we deleted four residues from the N-terminal portion of loop 2 (residues Asp595, Glu596, Glu597, and Lys598) to generate the DEEK MV 1IQ construct. The baculovirus system was used to express the myosin V and smooth muscle myosin constructs, which contained a C-terminal FLAG tag for purification purposes (*5*). All myosin V constructs were coexpressed with the essential light chain LC-1sa (*9*), and the smooth muscle myosin subfragment 1 (SmS1) constructs were coexpressed with the essential and regulatory light chains (*18*). The purity was greater than 95% based on Coomassie stained SDS gels. Myosin concentrations were determined using the Bio-Rad microplate assay (*5*).

Actin was purified from rabbit skeletal muscle using an acetone powder method (*20*) and gel filtered. Pyrene actin was generated by labeling actin with pyrene iodoacetamide (Molecular Probes) as described (*21*).

All experiments with myosin V were performed in KMg50 buffer (50 mM KCl, 1 mM EGTA, 1 mM $MgCl_2$, 1 mM DTT, and 10 mM imidozole-HCl, pH 7.0, 25 °C) and those with smooth muscle myosin in 20/20 buffer (20 mM MOPS, pH 7.0, 20 mM KCl, 1 mM EGTA, 5 mM $MgCl_2$, and 1 mM DTT) at 25 °C. Since SmS1 has a weaker affinity for actin, it was necessary to perform the actin-binding and steady-state ATPase experiments in 20/20 buffer.

Steady-State ATPase Activity of MV 1IQ. Steady-state ATP hydrolysis by MV 1IQ LC-1sa (50−100 nM) or SmS1 (200 nM) in the presence and absence of actin (0−40 μM) was examined using the NADH-linked assay (*9*) with a final MgATP concentration of 1 mM.

Stopped-Flow Measurements and Kinetic Modeling. Transient kinetic experiments were performed in a Applied Photophysics (Surrey, U.K.) stopped-flow with a dead-time of 1.2 ms. Tryptophan fluorescence was measured by exciting the sample at 295 nm, and the emission was measured using a 320 nm long pass filter. Pyrene actin was excited at 365 nm and mant-labeled nucleotides were excited at 295 nm, and their emission was measured using a 400 nm long pass filter.

The kinetics of phosphate release were measured using phosphate-binding protein covalently labeled with *N*-[2-(1-maleimidyl)ethyl}-7-(diethylamino)coumarin-3-carboxamide (MDCC-PBP) (generously provided by Steven Rosenfeld, University of Alabama) (*22*). The fluorescence of MDCC-PBP, which increases severalfold in the presence of inorganic phosphate (*22*, *23*), was excited at 425 nm, and the emission was measured through a 435 nm long pass filter. Phosphate release was measured with a sequential mix experiment in which 2 μM MV 1IQ was mixed 10 μM ATP and aged for 1 s to allow MV 1IQ to bind and hydrolyze the ATP, and then the MV·ADP·Pi complex was mixed with actin (0−45 μM), 5 μM MDCC-PBP, and 2 mM ADP (*24*) (final concentrations after mixing 0.5 μM MV 1IQ, 2.5 μM ATP, 5 μM MDCC-PBP, and 2 mM ADP). All solutions were preincubated with 7-methylguanosine (0.2 mM) and purine nucleoside phosphorylase (0.2 units·ml^{-1}) to remove background phosphate.

Nonlinear least-squares fitting of the data was done with software provided with the instrument or Kaliedagraph (Synergy Software, Reading, PA). Uncertainties reported are standard error of the fits unless stated otherwise.

Kinetic modeling and simulations were performed using the reaction scheme shown in Scheme 1), which has been used in recent kinetics studies of myosin V (*9*−*12*). In this scheme, myosin, actin, and actomyosin are represented by M, A, and AM, respectively. The rate and equilibrium constants are labeled on the basis of the reaction proceeding from left to right and those between the actin-associated and

Scheme 1

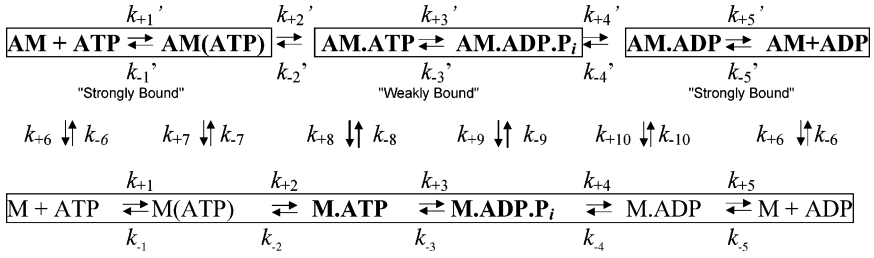

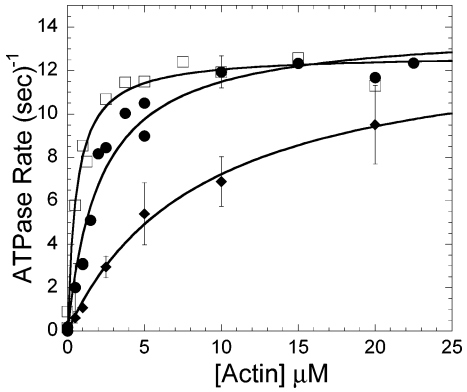

FIGURE 2: Steady-state ATPase of MV 1IQ constructs. The ATPase rate of WT MV 1IQ (●), LP2AAA MV 1IQ (◆), and DEEK MV 1IQ (□) were measured with the NADH-coupled assay and plotted as a function of actin concentration (myosin concentration 100 nM). The data were fit to the Michaelis−Menton equation to determine the V_{MAX} (maximum rate of ATP turnover) and K_{ATPase} (actin concentration at which there is half-maximal activation). The mean ATPase rate at each actin concentration determined from a least two separate myosin V preparations was plotted and fit to the Michaelis−Menton equation to determine V_{MAX} and K_{ATPase}. The error bars represent standard deviations of the mean ATPase rate at each actin concentration. The data are summarized in Table 1.

Table 1: Summary of Steady-State ATPase Results

construct	V_{MAX}[a] (mol of Pi·s^{-1}·(mol of myosin)$^{-1}$)	K_{ATPase}[b] (μM)
WT MV 1IQ	14.1 ± 1.1	2.2 ± 0.6
LP2AAA MV 1IQ	13.6 ± 1.0	8.8 ± 1.4
DEEK MV 1IQ	12.7 ± 0.3	0.6 ± 0.1

[a] Maximum rate of ATP turnover as determined from fitting the data in Figure 2 to the Michaelis−Menton equation. [b] Actin concentration at which the ATPase rate is one-half of the maximal rate also determined from fitting the data in Figure 2 to the Michaelis−Menton equation.

-dissociated steps proceeding in the dissociated direction. The main flux of the reaction pathway is shown in bold.

RESULTS

Steady-State ATPase Assays. The steady-state ATPase rates of WT and mutant MV 1IQ were plotted as a function of actin concentration and fit to the Michaels−Menton equation to determine the maximum rate of ATP turnover (V_{MAX}) and actin concentration at which the ATPase rates were one-half the maximal rate (K_{ATPase}) (Figure 2, Table 1). The average ATPase rate at each actin concentration determined from a least two separate myosin V preparations was plotted and fit to the Michaelis−Menton equation to determine V_{MAX} and K_{ATPase}. The K_{ATPase} of LP2AAA MV 1IQ was increased 4-fold (8.8 ± 1.4 μM) and the K_{ATPase} of DEEK MV 1IQ was reduced 3.7-fold (0.6 ± 0.1 μM) compared WT MV 1IQ (2.2 ± 0.6 μM), while the V_{MAX}'s of both mutants were very similar to WT MV 1IQ (13.6 ± 1.0, 12.7 ± 0.3, 14.1 ± 1.1 s^{-1}, respectively).

Table 2: Rate and Equilibrium Constants for ATP Binding and Hydrolysis

construct	K_1k_{+2}[a] (μM^{-1}·s^{-1})	$k_{+3} + k_{-3}$[a] (s^{-1})	$K'_1K'_{+2}$[b] (μM^{-1}·s^{-1})	K'_1[b] (μM)	k'_{+2}[b] (s^{-1})
WT MV 1IQ	1.6 ± 0.2	750 ± 30	1.6 ± 0.1	477 ± 44	771 ± 70
LP2AAA MV 1IQ	2.6 ± 0.2	680 ± 30	1.2 ± 0.1	718 ± 51	853 ± 20
DEEK MV 1IQ	1.9 ± 0.3	801 ± 77	1.9 ± 0.4	548 ± 125	1080 ± 89

[a] Measured with intrinsic tryptophan fluorescence in the absence of actin. [b] Measured with pyrene actin fluorescence.

The steady-state ATPase of monomeric LP2AA SmS1 at 60 μM actin (0.09 s^{-1}) was similar to the basal ATPase rate in the absence of actin (0.08 s^{-1}), while the WT SmS1 was activated severalfold (0.11 and 0.33 s^{-1}, respectively) at 37 °C in 20/20 buffer.

ATP Binding and Hydrolysis. The tryptopan fluorescence enhancement of MV 1IQ can be used to monitor the rates of both ATP binding and hydrolysis (*9*, *12*). Plots of the rate of the tryptophan fluorescence increase as a function of ATP concentration were fit to a hyperbola, and the extracted rate and equilibrium constants for ATP binding and hydrolysis are shown in Table 2. The second-order rate constant for ATP binding to MV 1IQ, determined from the initial slope of the hyperbola, was very similar in the WT and mutant MV 1IQ constructs ($K_1k_{+2} \approx 1-2$ μM^{-1}·s^{-1}). In addition, the effective rate constant of hydrolysis, determined from the maximum rate of the tryptophan fluorescence signal, was also very similar in the WT and mutant MV 1IQ constructs ($k_{+3} + k_{-3} \approx 700-800$ s^{-1}).

ATP-Induced Dissociation of acto-MV 1IQ. The ATP-induced dissociation of MV 1IQ from actin was monitored with pyrene actin fluorescence as described (*9*). Pyrene actin is quenched when myosin is strongly bound to actin and recovers when ATP-binding induces formation of the weakly bound actomyosin states. The data were fit to two exponentials with the fast phase modeled as the rate of ATP-induced dissociation and the slow phase as the rate of ADP release. The fast phase consisted of 90% of the total amplitude, while the slow phase was approximately 10% of the total amplitude. Thus, although the actomyosin sample was treated with apyrase, 10% of the MV 1IQ still had ADP bound prior to mixing with ATP. The rate of the slow phase was similar to the rate of mantADP release and the V_{MAX} from the steady-state ATPase assay. The rate of the fast phase of the pyrene fluorescence recovery was plotted as a function of ATP concentration and fit to a hyperbola (Figure 3) to determine the rate and equilibrium constants for ATP binding to acto-MV 1IQ (Table 2). The rates and equilibrium constants for ATP-induced dissociation of actomyosin V 1IQ were very similar in the WT and LP2AAA MV 1IQ constructs

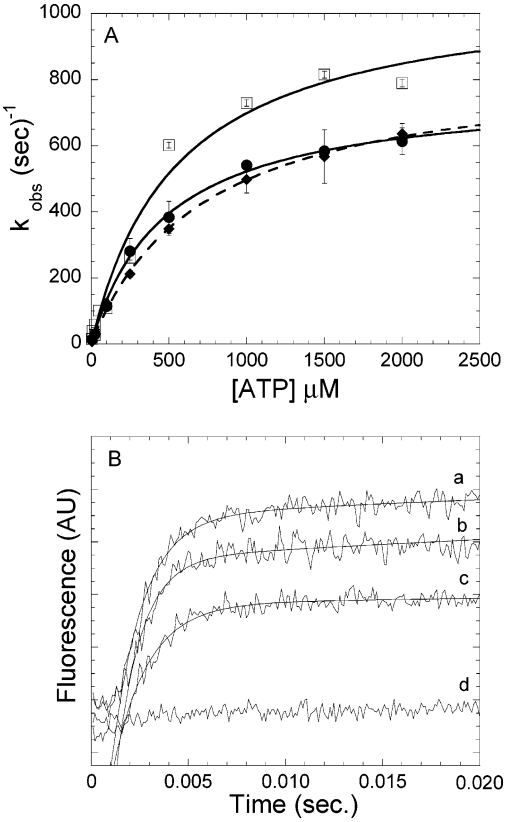

FIGURE 3: ATP-induced dissociation of acto-MV 1IQ. In panel A, the ATP-induced dissociation of acto-MV 1IQ (0.15 μM) (k_{obs}) and the ATP concentration dependence was determined for WT MV 1IQ (●), LP2AAA MV 1IQ (◆), and DEEK MV 1IQ (□). Points are the average of 1−3 transients, and error bars represent the standard errors of the fit to the averaged transient. Panel B presents time courses of ATP-induced dissociation of MV 1IQ constructs from pyrene actin. The fast phases of the time courses were 642 ± 29, 789 ± 36, and 585 ± 39 for (a) LP2AAA MV 1IQ, (b) DEEK MV 1IQ, and (c) WT MV 1IQ, respectively, and (d) the buffer control. Final reaction conditions were as follows: 0.15 μM pyrene actomyosin and 2 mM MgATP. The rate and equilibrium constants determined from the hyperbolic fits of the data and standard error from the fits are shown in Table 2.

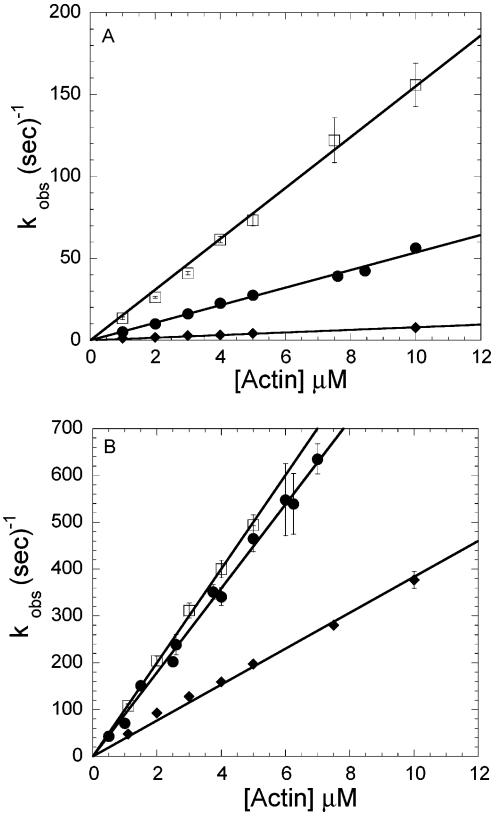

FIGURE 4: Binding of MV 1IQ to pyrene actin filaments. The rate (k_{obs}) of WT MV 1IQ (●), LP2AAA MV 1IQ (◆), or DEEK MV 1IQ (□) binding to pyrene actin filaments was determined by monitoring the rate of pyrene fluorescence quenching upon mixing MV 1IQ with 10-fold excess pyrene actin. Panel A shows that the rates of pyrene actin binding in the presence of 0.4 mM ADP were linearly dependent on actin concentration. Panel B shows that the rates of pyrene actin binding in the absence of nucleotide (apyrase-treated) were also linearly dependent on actin concentration. Points are the average of 1−3 transients, and error bars represent the standard errors of the fits. The rate and equilibrium constants determined from the linear fits to the data are shown in Table 3. Final reaction conditions were as follows: actin concentration as indicated, MV 1IQ concentration 10-fold lower than the actin, and 0.4 mM ADP.

(K'_1 = 477 ± 44 and 718 ± 51 μM, respectively, k'_{+2} = 771 ± 70 and 853 ± 20 s^{-1}, respectively, and $K'_1k'_{+2} \approx$ 1−2 $\mu M^{-1}\cdot s^{-1}$; see Table 2). However, the DEEK MV1IQ construct had a similar second-order rate constant and equilibrium constant for ATP-binding ($K'_1k'_{+2}$ = 1.9 ± 0.4 $\mu M^{-1}\cdot s^{-1}$ and K'_1 = 548 ± 125 μM, respectively) as described above but displayed a slightly faster maximum rate of ATP-induced dissociation (k'_{+2} = 1080 ± 89 s^{-1}) from pyrene actin than WT MV 1IQ.

Binding to Pyrene Actin Filaments. MV 1IQ binding to actin was measured by monitoring the rate of pyrene actin fluorescence quenching upon mixing MV 1IQ with 10-fold excess pyrene actin in the presence and absence of ADP. The rate of pyrene actin fluorescence quenching fit well to a single exponential and was linearly dependent on the actin concentration, in the range of actin concentrations measured (1−10 μM actin), for WT, LP2AAA, and DEEK MV 1IQ (Figure 4). A 5-fold reduction in the second-order rate constant for binding to pyrene actin in the presence of ADP was observed for the LP2AAA MV 1IQ (k_{-10} = 0.9 ± 0.1 $\mu M^{-1}\cdot s^{-1}$) construct compared to WT-MV 1IQ (k_{-10} = 5.5 ± 0.1 $\mu M^{-1}\cdot s^{-1}$), while a 3-fold increase in the second-order rate constant was observed for DEEK MV 1IQ (k_{-10} = 14.6 ± 0.4 $\mu M^{-1}\cdot s^{-1}$). Dissociation from pyrene actin, measured by mixing MV 1IQ bound to pyrene actin with 20-fold excess unlabeled actin, was 0.08 s^{-1} for WT and LP2AAA MV 1IQ and 0.04 s^{-1} for DEEK MV 1IQ.

We also measured the rate of MV 1IQ binding to pyrene actin as described above but in the absence of nucleotide. The second-order rate constant for LP2AAA MV 1IQ (k_{-6} = 38 ± 1 $\mu M^{-1}\cdot s^{-1}$) binding to pyrene actin was reduced 3-fold compared to WT MV 1IQ (k_{-6} = 90 ± 1 $\mu M^{-1}\cdot s^{-1}$), while the second-order rate constant for DEEK MV 1IQ (k_{-6} = 100 ±1 $\mu M^{-1}\cdot s^{-1}$) binding to actin was similar to WT MV 1IQ.

We also analyzed the actin binding properties of a smooth muscle myosin II loop 2 mutant (LP2AA SmS1) (*18*) that is similar to our LP2AAA myosin V mutant. We measured pyrene actin binding in the presence of ADP as described above for WT and LP2AA SmS1 (Figure 5). We measured the rate of SmS1 binding to actin, which was dependent on the actin concentration in a hyperbolic manner as described previously (*25*) and allowed us to obtain the maximum rate of binding to actin in the presence of ADP. Although it is

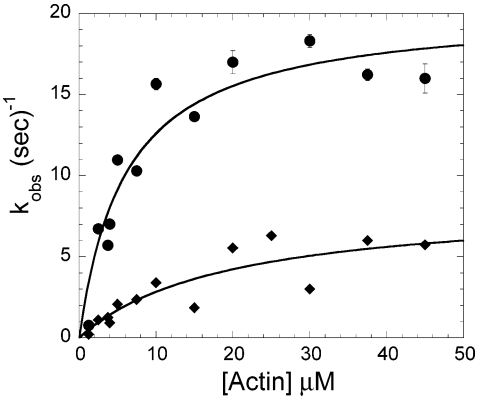

FIGURE 5: Binding of SmS1 to pyrene actin filaments. The rate (k_{obs}) of WT SmS1 (●) and LP2AA SmS1 (◆) binding to actin in the presence of ADP was determined as in Figure 4 except experiments were performed in 20/20 buffer. Points are the average of 1−3 transients, and error bars represent the standard errors of the fits. The rate and equilibrium constants determined from the hyperbolic fits are listed in the Results.

possible that the actin binding rates of MV 1IQ may also saturate in lower ionic strength 20/20 buffer, we were unable to perform the experiment because of protein aggregation problems of MV 1IQ in 20/20 buffer. The LP2AA SmS1 construct had a 2−3-fold reduced maximum rate of binding to actin compared to WT SmS1 (8.3 ± 2.3 and 20.3 ± 1.7 s^{-1}, respectively), and the actin concentration at which half-maximal saturation occurs was reduced 3-fold compared to WT SmS1 (6.1 ± 1.7 and 19.4 ± 11.6 μM, respectively). The second-order binding constant for LP2AA SmS1 binding to actin in the presence of ADP was reduced nearly 10-fold compared to WT SmS1 (0.4 ± 0.1 and 3.3 ± 0.7 $\mu M^{-1}\cdot s^{-1}$, respectively).

ADP Release from acto-MV 1IQ. The rate of ADP release from MV 1IQ in the presence of actin was determined by monitoring mant-ADP dissociation from acto-MV 1IQ upon mixing with excess unlabeled ADP (Figure 6). The rates of ADP release from acto-WT and -LP2AAA were very similar (15.1 ± 0.2 and 15.5 ± 0.1, respectively), while ADP release from acto-DEEK MV 1IQ was slightly increased (19.6 ± 0.8 s^{-1}) (Table 3). We also measured the rate of ADP release from acto-DEEK MV 1IQ by competition with ATP-induced dissociation from pyrene actin as described above (the slow phase of the biexponential fit to the data), which gave a rate (12 ± 0.8 s^{-1}) similar to the V_{MAX} from the steady-state ATPase assay. The ADP release rates for WT and LP2AAA MV 1IQ, determined as described above, were quite similar to the mant-ADP release rates (14 ± 1 and 17 ± 2, respectively).

Actin-Activated Phosphate Release. The release of phosphate from MV 1IQ was measured by performing a sequential mix experiment as described in Experimental Procedures. The fluorescence traces consisted of a fast single exponential phase (modeled to be the phosphate release rate) followed by a linear phase (modeled to be the steady-state turnover rate). The rate of phosphate release was hyperbolically dependent on actin concentration and reached a maximum that was similar in the WT, LP2AAA, and DEEK MV 1IQ constructs (k'_4 = 110 ± 10, 153 ± 75, and 101 ± 9 s^{-1}, respectively) (Figure 7A). However, the actin concentration at which half-maximal saturation was achieved (K_9) was increased 5-fold in the LP2AAA (51 ± 38 μM) compared to WT MV 1IQ (9 ± 2 μM), while DEEK MV 1IQ (3 ± 1 μM) was reduced nearly 5-fold compared to WT MV 1IQ. A slight variability in myosin concentration may have altered the linear phase of the phosphate release transients (Figure 7B).

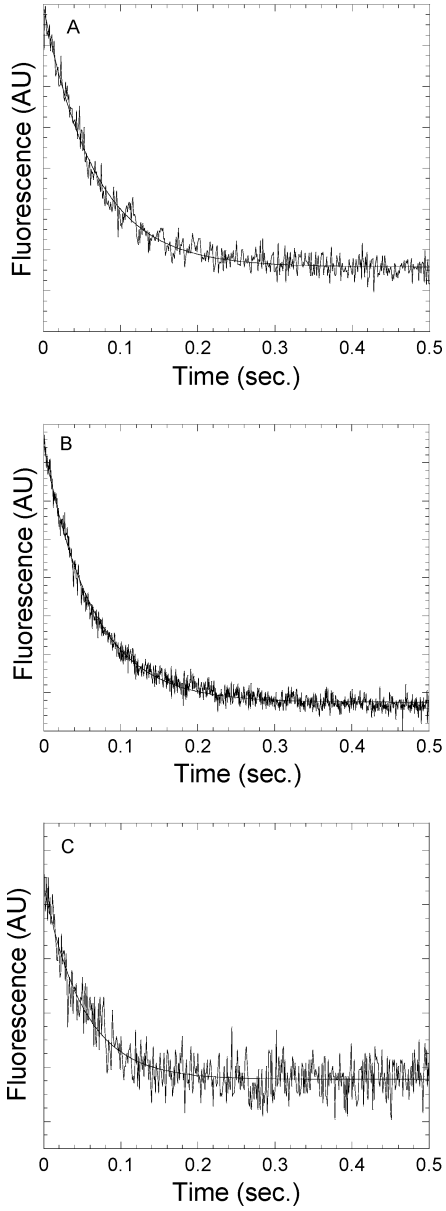

FIGURE 6: ADP release from acto-MV 1IQ. The rate of ADP dissociation from acto-MV 1IQ was measured by mixing acto-MV 1IQ (1 μM) bound to mant-ADP (10 μM) with excess unlabeled ADP (2 mM) (all concentrations listed are final). The rate of the fluorescence decrease was fit to a single exponential. The time courses for the mant-ADP release from WT (A), LP2AAA (B), and DEEK MV 1IQ (C) in the presence of actin and their corresponding single-exponential fits (15.1 ± 0.2, 15.5 ± 0.1, and 19.6 ± 0.8, respectively) are shown. The fluorescence traces are the average of 1−3 transients.

DISCUSSION

We have determined that loop 2 of myosin V plays an important role in myosin V's ability to bind actin with a relatively high affinity in the weak binding states. The modifications that we made to loop 2 of myosin V affected the actin-binding kinetics without significantly altering other steps in the actomyosin V ATPase cycle. In contrast, a similar

Table 3: Summary of Rate and Equilibrium Constants for Actin Binding and Product Release

construct	$k_{-10}{}^a$ ($\mu M^{-1}\cdot s^{-1}$)	$k_{+10}{}^a$ $(s)^{-1}$	$K_{10}{}^a$ (μM)	$k_{-6}{}^a$ ($\mu M^{-1}\cdot s^{-1}$)	$K_9{}^b$ (μM)	$k'_{+4}{}^b$ (s^{-1})	$k_{-5}{}^c$ (s^{-1})
WT MV 1IQ	5.5 ± 0.1	0.08	14.5 ± 0.1	90 ± 1	9 ± 2	110 ± 10	15.1 ± 0.2
LP2AAA MV 1IQ	0.9 ± 0.1	0.08	88.9 ± 0.1	38 ± 1	51 ± 38	153 ± 75	15.5 ± 0.1
DEEK MV 1IQ	14.6 ± 0.4	0.04	2.7 ± 0.4	100 ± 1	3 ± 1	101 ± 9	19.6 ± 0.8

[a] Measured with pyrene actin. [b] Measured with phosphate-binding protein. [c] Measured with mant-ADP.

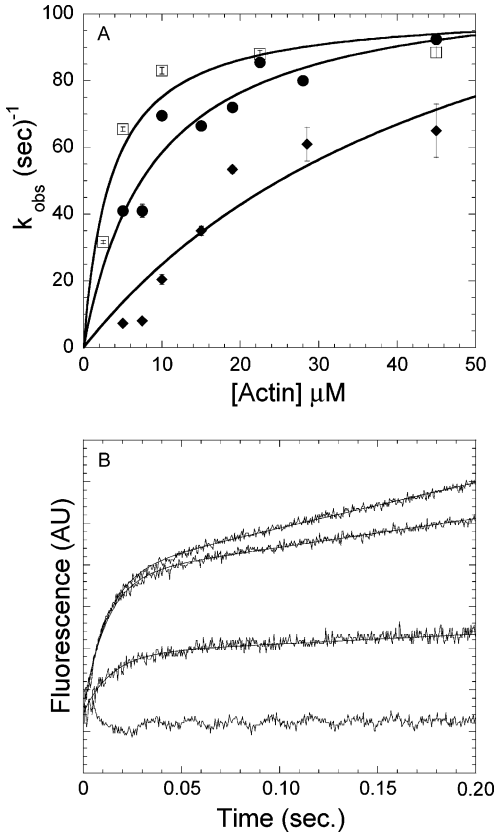

FIGURE 7: Actin-activated phosphate release from MV 1IQ constructs. The rate (k_{obs}) of phosphate release was measured by performing a sequential mix experiment and using phosphate-binding protein as an indicator of inorganic phosphate production as described in Experimental Procedures. In panel A, the rate of phosphate release was plotted as a function of actin concentration and fit to a hyperbola. The rate and equilibrium constants determined from the hyperbolic fits to the data are shown in Table 3. Points are the average of 1−3 transients, and error bars represent the standard errors of the fits. Panel B shows the time course of phosphate release from LP2AAA (lower trace), DEEK (upper trace), and WT MV 1IQ (middle trace) constructs in the presence of 45 μM actin. The time courses were fit to a single exponential with a slope (the values for the single-exponential fits were 65 ± 8, 89 ± 2, and 92 ± 2,for LP2AAA, DEEK and WT MV 1IQ, respectively). Final reaction conditions were as follows: 0.5 μM MV 1IQ, 5 μM PBP, indicated actin concentration, and 2 mM ADP.

mutation in smooth muscle myosin completely blocked its actin-activated ATPase activity and in vitro motility (*18*). Our results indicate that the net positive charge of loop 2 and not necessarily the size of the loop mediates the affinity of myosin V for actin in the weak binding states. Thus, the current study provides a structural mechanism for how myosin V contains a high affinity for actin in the weak binding states.

Kinetics of MV 1IQ Loop 2 Mutants. The results of the steady-state ATPase assays clearly demonstrate that the modifications that we made to loop 2 of myosin V altered the K_{ATPase} without changing the V_{MAX}. Substitution of three lysines to alanines in loop 2 (LP2 AAA MV 1IQ) increased the K_{ATPase}, indicating a weaker affinity for actin, and the deletion of four residues, three negatively charged and one positively charged, in loop 2 (DEEK MV 1IQ) reduced the K_{ATPase}, indicating a higher affinity for actin. Thus, the mutations made to loop 2 affected the affinity for actin without altering the rate-limiting step (ADP release).

We performed a complete kinetic analysis of the MV 1IQ loop 2 mutants to determine what steps in the ATPase cycle were altered compared to WT MV 1IQ. The rates of ATP binding and hydrolysis, measured with intrinsic tryptophan fluorescence, were quite similar in the mutant and WT MV 1IQ constructs (Table 2). In addition, the rates of ATP-induced dissociation, monitored with pyrene actin fluorescence, were also very similar in the mutant and WT MV 1IQ constructs. A slight increase in the maximum rate of dissociation (k'_{+2}) was observed with DEEK MV 1IQ. Perhaps a rearrangement of loop 2 is necessary to allow dissociation from actin, and the shorter loop can more efficiently undergo this conformational change.

Our results demonstrate that modifying the structure of loop 2 dramatically alters the actin binding kinetics of myosin V. We directly measured MV 1IQ binding to pyrene actin in the presence and absence of ADP. As demonstrated previously (*9*), the rate of myosin V binding to pyrene actin was linearly dependent on actin concentration in both the presence and absence of ADP (Figure 3). The results of the actin binding experiments with LP2 AAA MV 1IQ suggest that the three lysine residues in loop 2 are important determinants of the rate of association with actin in both the ADP and rigor states. The 5-fold reduction in the affinity of LP2AAA MV 1IQ for actin in the presence of ADP was solely due to the reduced actin association rate since the rate of dissociation was unaffected by the mutation. In contrast, the DEEK MV 1IQ construct had a 3-fold faster rate of binding to pyrene actin in the presence of ADP compared to WT MV 1IQ but was similar to WT MV 1IQ in the absence of nucleotide. The rate of binding to actin in the absence of nucleotide is extremely fast, approaching the diffusion-limited rate of binding (*9*), and therefore it is perhaps not surprising that the DEEK MV 1IQ mutant did not enhance this rate further. Overall, our results suggest that the number of positively charged amino acids in loop 2 of myosin V correlates with the rate of association with actin. Our results agree with previous reports that have determined the net positive charge of loop 2 of myosin II controls the rate of binding to actin (*16*). In addition, the removal of the first part of the unique actin-binding insert in myosin V does not appear to be critical for binding to actin. These results are consistent with the smooth muscle myosin mutant with 16 amino acids deleted from loop 2, which enhanced its apparent affinity for actin without affecting other steps in

the myosin ATPase cycle (*18*). Thus, the size of loop 2 may not be as critical as the net positive charge of the loop or perhaps the position of the positive charges, which play a role in modulating the affinity of myosin for actin.

We examined the actin binding kinetics of the LP2AA SmS1, which when examined in the dimeric HMM construct was shown to contain very little actin-activated ATPase activity or in vitro motility (*18*). Our results demonstrated a 10-fold reduction in the actin association rate and a 2−3-fold reduction in the maximum rate of LP2AA SmS1 binding to actin in the presence of ADP compared to WT SmS1. Since the rate of binding to actin in the presence of ATP is even slower, the LP2AA SmS1 mutant may indirectly block actin activation of phosphate release by reducing the rate of entry into the strong binding state. This would explain the single molecule experiments performed with the smooth muscle myosin lysine mutant, which demonstrated that the frequency of events observed was reduced 20-fold (i.e., the probability of binding strongly to actin) while the lifetimes of the events were similar to WT SmS1 (the length of time myosin is bound to actin) (*26*). The corresponding mutation in myosin V, LP2AAA MV 1IQ, may be much less severe because myosin V has a much faster rate of binding to actin in the presence of ATP than myosin II. Overall, these results highlight a key kinetic difference between myosin V and myosin II in that the transition from a weak to a strong actin-binding conformation is greatly accelerated in myosin V.

Product Release Steps. De La Cruz et al. (1999) demonstrated that the K_{ATPase} of myosin V can be expressed as a function of the following rate and equilibrium constants.

$$K_{ATPase} = k'_{+5}/(K_9 k'_{+4})(K_3/(K_3 + 1))$$

In both the mutant and WT MV 1IQ constructs, the V_{MAX} and ADP release rate (k'_{+5}) were quite similar, and the rate of ATP hydrolysis ($k_{+3} + k_{-3}$) was very similar, suggesting that the equilibrium constant for ATP hydrolysis (K_3) was unaffected. Therefore, our results suggest that the changes observed in the K_{ATPase} of the loop 2 mutants were due to changes in K_9, k'_{+4}, or both. The results shown in Figure 5 clearly demonstrate that the maximum rate of phosphate release (k'_{+4}) was similar in the loop 2 mutant and WT MV 1IQ constructs, but the actin concentration dependence (K_9) on the rate of phosphate release was dramatically altered. The calculated K_{ATPase} of the WT and mutant MV 1IQ constructs using the above formula and our measured rate and equilibrium constants is in good agreement with the measured K_{ATPase} in our steady-state ATPase experiments, providing further evidence for the validity of the formula proposed by De La Cruz and colleagues (1999). The maximum rate of phosphate release measured for WT MV 1IQ in the current study was different than that measured by De La Cruz et al. (*9*), but it is unclear what the cause of this difference is. However, our results agree within a factor of 2 of the previous report and do not conflict with the overall conclusion that phosphate release is quite rapid in myosin V and ADP release is rate-limiting (*9*). Nonetheless, the current results suggest that the affinity for actin in the M·ADP·Pi state ($K_9 = 9 \pm 2$ μM) is higher than that of conventional myosin II, which is consistent with our previous report that demonstrated a high actin affinity in the M·ATP state (*11*). Interestingly, by reducing the number of positive charges in loop 2 of myosin V, such as in LP2AAA MV 1IQ, the affinity for actin can be reduced to a value that is more like that of conventional myosin II. The high affinity for actin in the M·ADP·Pi state, which is enhanced by the large number of positively charged amino acids in loop 2 (net positive charge of +5), may be critical for allowing myosin V to move processively along actin (*24*).

The results from the phosphate release and ADP release experiments suggest that loop 2 does not play a role in actin activation of product release in myosin V. Our results support previous reports that demonstrated that loop 2 modulates the affinity for actin without significantly altering the maximum rate of ATPase activity (*13, 14*). Conversely, mutagenesis of loop 2 in *Dictyolstelium* myosin II demonstrated that loop 2 is involved in activating ADP and phosphate release (*4, 15−17*). In addition, adding three lysines residues to loop 2 of smooth muscle myosin reduced the rate of ADP release while not changing the maximum ATPase rate (*27*). Thus, it is possible that the effects of loop 2 on product release are myosin isoform specific, but the role of loop 2 in binding to actin is conserved throughout the myosin superfamily.

The positively charged amino acids in loop 2 may play a role in actin binding by mediating the initial interaction between actin and myosin. The positively charged amino acids in loop 2 likely interact with the highly negatively charged N-terminus of actin. Indeed, mutating or deleting several acidic residues in the N-terminal region of actin dramatically changed myosin binding affinity but did not completely block actin activation of myosin ATPase activity (*28*). Thus, interactions between loop 2 and the N-terminus of actin may provide the initial electrostatic steering between actin and myosin, which allows the formation of other hydrophobic and ionic interactions to generate the strongly bound actomyosin complex. Our results suggest the primary role of loop 2 in myosin V is to modulate the weak binding affinity. Since myosin V moves processively along actin taking 36 nm steps, its highly charged loop 2 may be important to allow one head to find the next actin binding site before the other head detaches.

In conclusion, we have revealed that loop 2 of myosin V plays an important role in allowing myosin V to bind actin with a relatively high affinity in the weak binding states. The net positive charge and not the size of loop 2 appears to be critical for myosin V's high-affinity actin binding. In contrast to studies on myosin II, loop 2 does not play a direct role in actin activation of product release in myosin V. Thus, the large and highly charged loop 2 of myosin V has kinetically tuned myosin V to increase its affinity for actin, which may be important for its ability to move processively along actin and function as an organelle transporter.

ACKNOWLEDGMENT

We thank Steven Rosenfeld for generously providing the phosphate-binding protein. We also thank E. Michael Ostap and Carl Morris for their comments and careful reading of this manuscript. We also recognize the excellent technical work of Corey Baldacchino and Jocelyn Nolt.

REFERENCES

1. Sellers, J. R. (1999) *Myosins*, 2nd edition, Protein Profile, Oxford University Press, Oxford, U.K.

2. Geeves, M. A., and Holmes, K. C. (1999) *Annu. Rev Biochem. 68*, 687−728.
3. Spudich, J. A. (1994) *Nature 372*, 515−518.
4. Uyeda, T. Q. P., Ruppel, K. M., and Spudich, J. A. (1994) *Nature 368*, 567−569.
5. Sweeney, H. L., Rosenfeld, S. S., Brown, F., Faust, L., Smith, J., Xing, J., Stein, L. A., and Sellers, J. R. (1998) *J. Biol. Chem. 273*, 6262−6270.
6. Murphy, C. T., and Spudich, J. A. (2000) *J. Muscle Res. Cell Motil. 21*, 139−151.
7. Mehta, A. D., Rief, M., Spudich, J. A., Mooseker, M. S., and Cheney, R. E. (1999) *Nature 400*, 590−593.
8. Reck-Peterson, S. L., Provance, D. W., Jr., Mooseker, M. S., and Mercer, J. A. (2000) *Biochim. Biophys. Acta 1496*, 36−51.
9. De La Cruz, E. M., Wells, A. L., Rosenfeld, S. S., Ostap, E. M., and Sweeney, H. L. (1999) *Proc. Natl. Acad. Sci. U.S.A. 96*, 13726−13731.
10. De La Cruz, E. M., Wells, A. L., Sweeney, H. L, and Ostap, E. M. (2000) *Biochemistry 39*, 14196−14202.
11. De La Cruz, E. M., Sweeney, H. L. and Ostap, E. M. (2000) *Biophys. J. 79*, 1524−1529.
12. Yengo, C. M. De La Cruz, E. M., Safer, D., Ostap, E. M., and Sweeney, H. L. (2002) *Biochemistry 41*, 8508−8517.
13. Rovner, A. S., Freyzon Y., and Trybus, K. M. (1995) *J. Biol. Chem. 270*, 30260−30263.
14. Rovner, A. S. (1998) *J. Biol. Chem. 273*, 27939−27944.
15. Murphy, C. T., and Spudich, J. A. (1999) *Biochemistry 38*, 3785−3792.
16. Furch, M., Geeves, M. A., and Manstein, D. J. (1998) *Biochemistry 37*, 6317−6326.
17. Knetsch, M. L. W., Uyeda, T. Q. P., and Manstein, D. J. (1999) *J. Biol. Chem. 274*, 20133−20138.
18. Joel, P. B., Trybus, K. M., and Sweeney, H. L. (2001) *J. Biol. Chem. 276*, 2998−3003.
19. Hiratsuka, T. (1983) *Biochim. Biophys. Acta 742*, 496−508.
20. Pardee, J. D., and Spudich, J. A. (1982) *Methods Enzmol. 85*, 164−181.
21. Pollard, T. D. (1984) *J. Cell Biol. 99*, 769−777.
22. Brune, M., Hunter, J. L., Corrie, J. E., and Webb, M. R. (1994) *Biochemistry 33*, 8262−8271.
23. White, H. D., Belknap, B., and Webb, M. R. (1997) *Biochemistry 36*, 11828−11836.
24. De La Cruz, E. M., Ostap, E. M., and Sweeney, H. L. (2001) *J. Biol. Chem. 276*, 32373−32381.
25. Rosenfeld, S. S., Xing, J., Cheung, H., Brown, F., Kar, S., and Sweeney, H. L. (1998) *J. Biol. Chem. 273*, 28682−28690.
26. Baker, J. E., Brosseau, C., Joel, P. B., and Warshaw, D. M. (2002) *Biophys. J. 82*, 2134−2147.
27. Joel, P. B., Sweeney, H. L., and Trybus, K. M. (2003) *Biochemistry 42*, 9160−9166.
28. Miller, C. J., Wenise, W. W., Bobkova, E., Rubenstein, P. A., and Reisler, E. (1996) *Biochemistry 35*, 16557−16565.

BI035510V